LETTER

Impacts of the north and tropical Atlantic Ocean on the Antarctic Peninsula and sea ice

Xichen Li[1], David M. Holland[1], Edwin P. Gerber[1] & Changhyun Yoo[1]

In recent decades, Antarctica has experienced pronounced climate changes. The Antarctic Peninsula exhibited the strongest warming[1,2] of any region on the planet, causing rapid changes in land ice[3,4]. Additionally, in contrast to the sea-ice decline over the Arctic, Antarctic sea ice has not declined, but has instead undergone a perplexing redistribution[5,6]. Antarctic climate is influenced by, among other factors, changes in radiative forcing[7] and remote Pacific climate variability[8,9], but none explains the observed Antarctic Peninsula warming or the sea-ice redistribution in austral winter. However, in the north and tropical Atlantic Ocean, the Atlantic Multidecadal Oscillation[10,11] (a leading mode of sea surface temperature variability) has been overlooked in this context. Here we show that sea surface warming related to the Atlantic Multidecadal Oscillation reduces the surface pressure in the Amundsen Sea and contributes to the observed dipole-like sea-ice redistribution between the Ross and Amundsen–Bellingshausen–Weddell seas and to the Antarctic Peninsula warming. Support for these findings comes from analysis of observational and reanalysis data, and independently from both comprehensive and idealized atmospheric model simulations. We suggest that the north and tropical Atlantic is important for projections of future climate change in Antarctica, and has the potential to affect the global thermohaline circulation[6] and sea-level change[3,12].

Recent multidecadal changes in Antarctic climate are well documented. Surface air temperature (SAT) in the Antarctic Peninsula[2,13], at the Faraday/Vernadsky station in particular, reveals a rapid warming trend of 5.6 K over 50 years in austral winter[1]. The accelerated land-ice melting around the Antarctic Peninsula and the Amundsen Sea[3,4] indicates enhanced warm air advection[3] and warm water transport to these regions[4]. Satellite observations show a dipole-like change in sea-ice concentration[5,6] (SIC), with increases in the Ross Sea[14] and decreases in the Amundsen–Bellingshausen–Weddell seas[6].

These regional-scale, multidecadal changes in Antarctica are strongly influenced by the atmospheric circulation[1,7]. During austral summer, Antarctic changes have been attributed to greenhouse gas increase[7] and stratospheric ozone loss[7,15,16], both of which project strongly onto the Southern Annular Mode[17,18]. In winter, however, the mechanisms driving Antarctic changes are less well understood. Previous studies have linked winter Antarctic climate variability to Pacific sea surface temperature (SST) variability, including the El Niño/Southern Oscillation[8,9] (ENSO) and central Pacific Ocean warming[19]. It is unclear, however, whether Pacific SST can explain Antarctic multidecadal climate changes. The ENSO does not exhibit significant multidecadal trends and therefore cannot account for recent Antarctic climate changes, and central Pacific warming appears to cool the Antarctic Peninsula and increase SIC over the Amundsen–Bellingshausen seas[19], in contrast to observed trends[1,2,5,6,14].

In comparison, the influence of the Atlantic Ocean has received less attention, although recent studies correlating Antarctic SAT with global SSTs have suggested potential links between Antarctic SAT and the south[2] and tropical[20] Atlantic. In this study, we single out north and tropical Atlantic SST as a key driver of recent Antarctic climate changes in austral winter, explaining both the Antarctic Peninsula warming and the SIC redistribution. Using observational data and numerical simulation, we demonstrate a teleconnection between the north and tropical Atlantic and Antarctica, and reveal the physical mechanism underlining this connectivity.

On decadal timescales, the Atlantic Multidecadal Oscillation[10,21] is a leading mode of global variability. Monthly mean north Atlantic SST variability since 1870 is dominated by a centennial warming (Fig. 1a) and a 60–70-year oscillation[10] (Fig. 1b). The Atlantic Multidecadal Oscillation is observed in SST reconstructions[10], palaeo-records[22] and millennial-scale climate simulations[21,23]. It has been associated with changes in the oceanic global thermohaline circulation[21,23], but may also be influenced by changes in atmospheric blocking[24] and anthropogenic forcing associated with the indirect aerosol effect[11,25]. The Atlantic Multidecadal Oscillation spatial pattern (Fig. 1e) exhibits two local maxima, one south of Greenland and one in the tropical Atlantic. To distinguish further the role of the tropical Atlantic, time series from this region alone are considered alongside north Atlantic SSTs in Fig. 1c. Tropical Atlantic SSTs are highly correlated ($R = 0.77$) with north Atlantic SSTs.

In the satellite era, from 1979 onwards, the Atlantic Multidecadal Oscillation manifests itself as an upward trend in north Atlantic SSTs, which, in combination with anthropogenic forcing, has led to a warming of more than half a degree (Fig. 1c). Although this positive trend gives the Atlantic Multidecadal Oscillation the potential to drive Antarctic climate changes, it complicates the assessment of the Atlantic Multidecadal Oscillation's impact in Antarctic observational records. To circumvent this limitation, we focus on detrended Atlantic SSTs (Fig. 1d), hereafter referred to as sub-decadal variability. Because these sub-decadal anomalies are slow relative to the timescales of the atmospheric wave propagation (Extended Data Fig. 1) but faster than the oceanic thermohaline circulation, we use them to identify the atmospheric fingerprint associated with warming in the north and tropical Atlantic. This is achieved by independent methods including regression, maximum covariance analysis (MCA) and numerical simulations.

Regression of austral winter (June, July and August) sea-level pressure (SLP) onto the north and tropical Atlantic SST time series (Fig. 2a, b) reveals a teleconnection between the Atlantic and Antarctica. Atlantic warming leads to dipolar changes in SLP, with increases south of Australia and decreases over Antarctica, in particular in the Amundsen Sea Low region. It therefore bears some resemblance to the positive phase of the Southern Annular Mode, with a pattern correlation of 0.84. The anomaly is barotropic, extending from the surface up to 200 hPa (Extended Data Fig. 2). A similar teleconnection is observed in all seasons except austral summer (Extended Data Fig. 3).

We independently identify this teleconnection between Atlantic SST and Southern Hemisphere SLP (Fig. 2c–e) through MCA. The first mode captures 55% of the squared covariance, and reveals a SLP spatial pattern (Fig. 2c) similar to the regression patterns (Fig. 2a, b). The SST pattern (Fig. 2d) is comparable to the Atlantic Multidecadal Oscillation, with broad warming across the north Atlantic and a bi-centre structure. The SST time series (Fig. 2e) is highly correlated ($R = 0.85$) with Atlantic sub-decadal variability (Fig. 1d). MCA thus simultaneously

[1]Courant Institute of Mathematical Sciences, New York University, 251 Mercer Street, New York, New York 10012, USA.
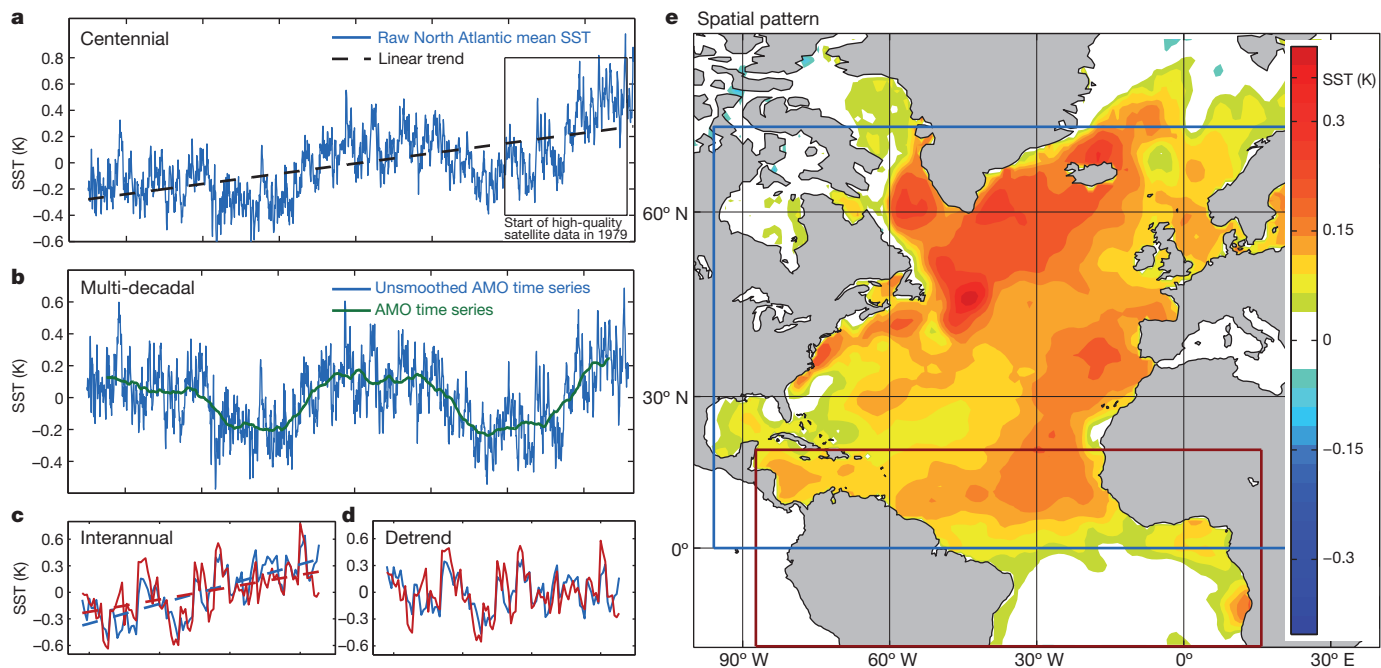
Figure 1 | Temporal variability of north and tropical Atlantic sea surface temperature anomalies at different timescales, and the spatial pattern of the Atlantic Multidecadal Oscillation. a, Area-weighted monthly mean SST in the north Atlantic ($0°$ N–$70°$ N) since 1870. The grey dashed line indicates the centennial trend. **b**, The blue curve shows mean SST after removing the linear trend signal and the green curve indicates the Atlantic Multidecadal Oscillation index, defined as a ten-year smoothed mean of the detrended time series. **c**, 1979–2012 (black box in **a**) austral winter monthly mean SST time series. The blue (or red) curve shows mean SST over the north (or tropical) Atlantic. The north (or tropical) Atlantic region is defined by the blue (or red) rectangle in

e; the Pacific sector inside each box is excluded. The linear trends are indicated by the dashed lines in **c**, which are a superposition of the global warming trend in **a** and the ascending Atlantic Multidecadal Oscillation index in **b**. **d**, The detrended time series of **c** serve as indices of the north and tropical Atlantic sub-decadal variability and are used in regression. **e**, The spatial pattern of the Atlantic Multidecadal Oscillation, defined as the normalized regression of north Atlantic SST (1870–2012) against the Atlantic Multidecadal Oscillation index, exhibiting two warm centres, one south of Greenland and one in the tropics.

reproduces the Atlantic Multidecadal Oscillation pattern and associates it with the Antarctic SLP teleconnection.

We establish a causal link between Atlantic SSTs and the Antarctic SLP pattern with numerical simulations using the Community Atmosphere Model (CAM4), a state-of-the-art atmospheric model (see Methods for details). The simulated SLP response to north (Fig. 2f) and tropical (Fig. 2g) Atlantic warming is comparable to the SLP pattern obtained from regression and MCA. The model reproduces the amplification of the Amundsen Sea Low, albeit with an eastward shift.

The simulation results suggest that warming in the tropical Atlantic generates the bulk of the SLP response to the whole Atlantic Multidecadal Oscillation pattern (Fig. 2f, g). The SLP response to warming in the mid-latitude north Atlantic is comparatively weaker (Extended Data Fig. 4). The SLP response to the Atlantic Multidecadal Oscillation can be viewed as a linear combination of the responses to mid-latitude north and tropical Atlantic warming, with the latter playing the key part.

Geostrophic balance connects SLP changes to surface wind anomalies, which affect regional-scale changes in SIC and SAT[6,14,26]. Regression of SLP, SIC and SAT onto tropical Atlantic sub-decadal variability (Fig. 3a) reveals the impact of the atmospheric teleconnection on Antarctic SIC and SAT. In particular, the low-pressure anomaly in the Amundsen Sea induces a cyclonic (clockwise) circulation, heating the Antarctic Peninsula by warm-air advection[14] (red arrows in Fig. 3a). Changes in thermal advection and wind-stress forcing associated with surface wind anomalies drive a SIC dipole redistribution[6,26]. Local feedbacks between the sea ice and the ocean may considerably amplify the initial response triggered by the wind forcing[27,28].

To assess the statistical significance of the SIC and SAT patterns associated with Atlantic SSTs, we must also take into account the spatial structure of the response. The aggregated SIC increase across the Ross

Sea, the SIC loss in the Amundsen–Bellingshausen–Weddell seas, and the SAT warming of the Antarctic Peninsula are statistically significant (see Methods and Extended Data Fig. 8).

Thus far we have established a climatic fingerprint of Atlantic warming on Antarctic climate (Fig. 3a) from sub-decadal variability. Because the timescales of the atmospheric circulation are fast relative to sub-decadal oceanic variability, the multidecadal response of Antarctic climate to Atlantic warming may also exhibit the same fingerprint. Multidecadal changes of SIC and SAT are shown in Fig. 3b. Reanalysis SAT is potentially biased over Antarctica[29], so we also include ground station SAT trends. SIC exhibits expansion around Antarctica, accompanied with a dipole redistribution between the Ross Sea and the Amundsen–Bellingshausen–Weddell seas[6,14] that is consistent with a deepening of the Amundsen Sea Low[14,18]. Both station observations and reanalysis SAT indicate a strong warming signal over the Antarctic Peninsula[1], although the cooling signal over Marie Byrd Land in the regression differs from observations[30], indicating that Atlantic SST changes do not explain the entire spatial pattern of west Antarctic warming. In east Antarctica, regression results (Fig. 3a) agree with station observations (Fig. 3b), both revealing a mild cooling trend. The reanalysis (Fig. 3b) indicates a warming tendency, but may be biased by surface energy balance errors[29].

A comparison of Fig. 3a and Fig. 3b reveals a strong resemblance between the sub-decadal fingerprint and the multidecadal changes in SIC and SAT. The SIC and SAT anomalies in Fig. 3a are associated with one standard deviation of the Atlantic SST variability, which is approximately 0.2 K. The net warming trend in the tropical Atlantic during the period 1979–2012, however, is approximately 0.5 K. Assuming a linear relationship between Atlantic SST and SIC/SAT, the amplitude of the fingerprint in Fig. 3a should be scaled by a factor of two, thus making it comparable to the multidecadal changes (Fig. 3b).
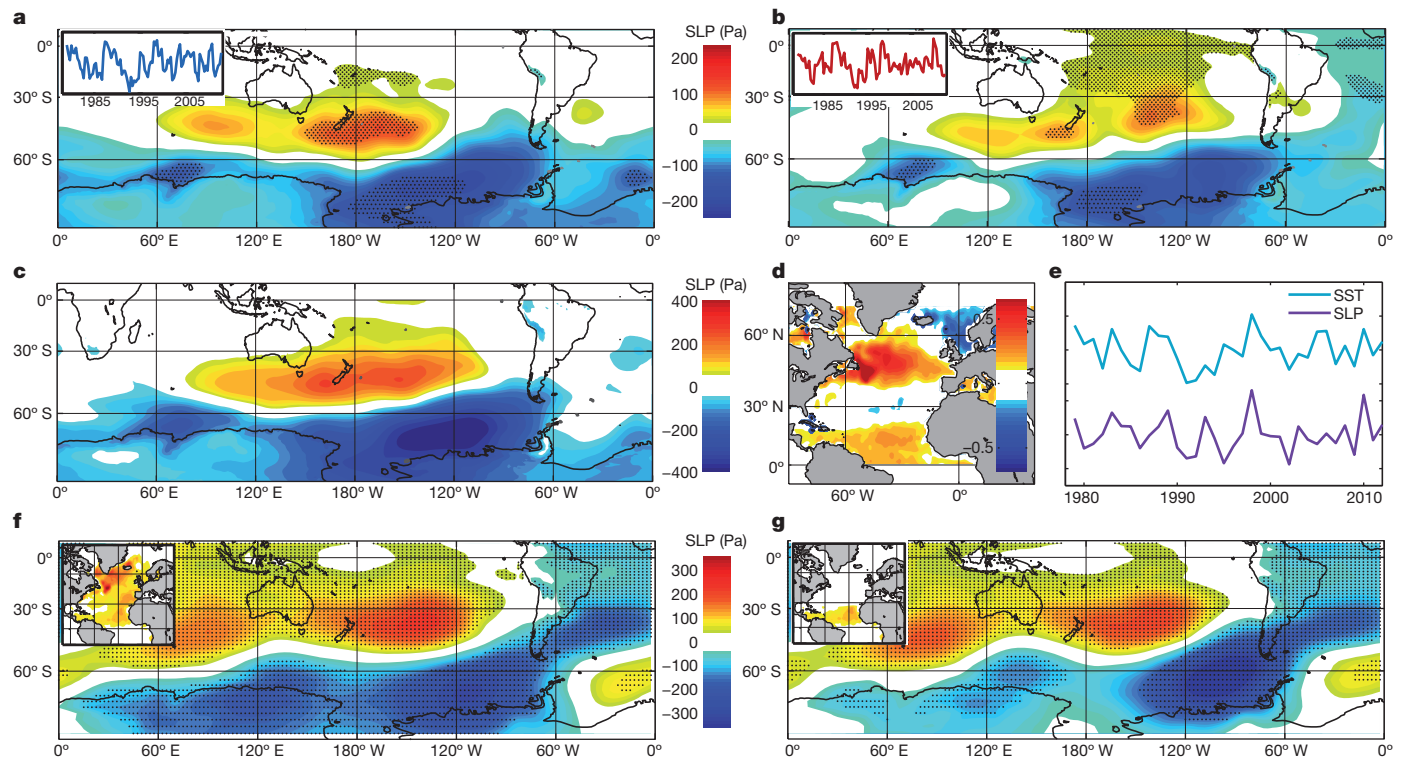
Figure 2 | North and tropical Atlantic variability projected onto austral winter Southern Hemisphere SLP by three independent analyses. a, b, The normalized regression of SLP against north Atlantic SST (**a**; the inset shows the time series) and tropical Atlantic SST (**b**). Areas of >95% significance (Student's *t*-test) are marked by black dots, restricted to the shaded regions. **c–e,** The first mode of MCA, including the spatial patterns of SLP (**c**) and SST (**d**), as well as their time series (**e**; unit free). **f, g,** Simulated SLP anomaly response to north Atlantic SST warming (**f**; the inset shows SST forcing) and tropical Atlantic SST warming (**g**; the inset shows SST forcing). The three analyses (**a**, **c** and **f**) show a coherent spatial pattern, suggesting a robust link between north Atlantic warming and Antarctic SLP and circulation anomalies. Evidence from simulation (**f, g**) implies an impact and causality coming from both the north and tropical Atlantic.
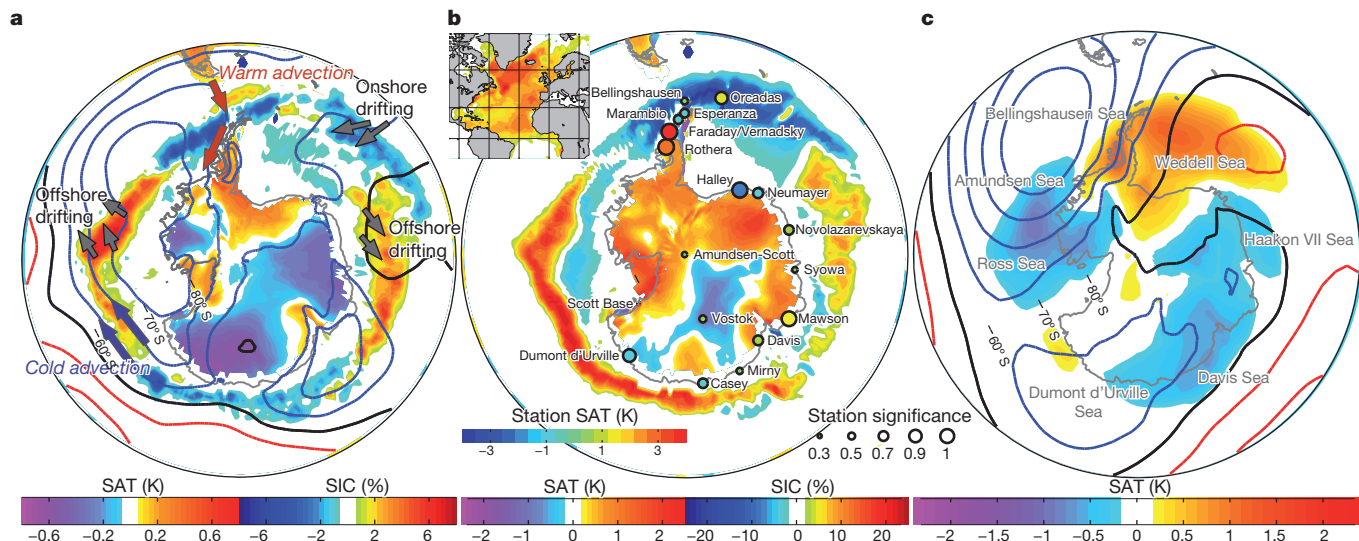

Figure 3 | The austral winter patterns of Antarctic SLP, SAT and SIC related to tropical Atlantic SST warming. a, SLP (red and blue contours indicate positive and negative anomalies respectively, 40 Pa interval), SAT (land-area colour) and SIC (ocean-area colour), individually regressed against the normalized tropical Atlantic SST. The regression on the north Atlantic SST shows similar signals, not shown. Atlantic SST-induced SAT/SIC patterns are consistent with SLP, via the mechanisms of thermal advection (red/blue arrows) and mechanical stress forcing (grey arrows). **b,** Epochal differences (1996–2012 minus 1979–1995) of SIC and SAT. SAT observations from 18 stations are also superimposed (circles, with colour showing the trends, and size corresponding to significance level). The Atlantic Multidecadal Oscillation spatial pattern is shown in the upper left. The similarity between sub-decadal variability (**a**) and multidecadal trends (**b**) implies a teleconnection between the Atlantic Multidecadal Oscillation and recent Antarctic climate change. The epochal difference of SLP is not shown in **b** because there exist uncertainties in the SLP reanalysis data. **c,** Simulated SLP (contours with 80 Pa interval) and SAT (colour) response to tropical Atlantic SST forcing (SIC is not included in the simulation) reveals causality in the above teleconnection.

The CAM4 simulations also suggest that the observed trend in SAT is a consequence of the circulation changes driven by tropical Atlantic warming. The SLP and SAT response to climatological tropical Atlantic SST forcing in CAM4 (Fig. 3c) nearly matches the regression results (Fig. 3a) and observed multidecadal trends (Fig. 3b). The amplitude of the CAM4 SAT patterns, however, should be interpreted with some caution. SAT in the polar region is affected by SIC changes, so the total response triggered by the atmospheric circulation change may depend on air–sea-ice–ocean interactions that are missing from our atmosphere-only model.

Remarkably, the SLP, SAT and SIC patterns obtained from sub-decadal regression, multidecadal observational trends and atmospheric model simulations all reveal a similar teleconnection between the north and tropical Atlantic and Antarctica. The regression and MCA results were derived using detrended, sub-decadal variability, and thus cannot independently inform us about multidecadal trends. However, given that the timescales of atmospheric variability are fast compared to sub-decadal climate variability, this sub-decadal teleconnection may imply the existence of a multidecadal link. The coherence between the multi-decadal trend (Fig. 3b) and detrended sub-decadal regression (Fig. 3a) significantly strengthens this argument, and the model simulations (Fig. 3c) establish causality, showing that Atlantic Multidecadal Oscillation SST forcing is a key driver of recent Antarctic climate change.

The mechanism by which tropical SSTs drive Antarctic atmospheric circulation depends critically on poleward propagating Rossby wave trains[8]. (Rossby waves are large-scale atmospheric wave structures that arise from variations in the effect of planetary rotation with latitude.) A similar physical process has been examined in previous studies[9,19], but focusing only on the tropical Pacific. In contrast, we simulate Rossby wave trains driven by tropical Atlantic SSTs (Fig. 2f, g and Extended Data Fig. 1g). CAM4 is a comprehensive atmospheric model that includes a wide array of physical processes, so it is difficult to isolate pure Rossby wave dynamics unambiguously. To focus on these dynamics alone, we performed idealized simulations with the 'dry dynamical core' of a Geophysical Fluid Dynamics Laboratory (GFDL) atmospheric model (see Methods for details). Using austral winter background conditions (Extended Data Fig. 1a–f), we demonstrate that convective heating over the tropical Atlantic generates Rossby wave trains that propagate around the globe within two weeks, ultimately focusing on and enhancing the Amundsen Sea Low. This wave pattern matches well with CAM4 simulations (Extended Data Fig. 1g), and further establishes that Rossby wave trains directly link the tropical Atlantic to Antarctica.

Although we have used subdecadal variability to identify the tele-connection from the north and tropical Atlantic to the Antarctic region, it is important to note that Pacific SST variability—the ENSO in particular—dominates the interannual variability of Antarctic climate[8,9,27]. The Atlantic, however, becomes a dominant driver of Antarctic climate on multidecadal timescales (see Methods and Extended Data Fig. 6).

In addition to the demonstrated impacts on SAT and SIC, this study implies broader impacts of north and tropical Atlantic warming, specifically on global sea-level change and the thermohaline circulation. The dramatic breakup of the Larsen A and B ice shelves and the present thinning of the C shelf have been attributed to atmospheric thermal advection[3], shown in this study to be driven, in part, by north and tropical Atlantic warming. These surface land-ice changes, in conjunction with basal melting processes caused by sub-ice-shelf intrusion of warm water, are contributing to an accelerated global sea-level rise[12]. Additionally, the SAT and SIC in the Weddell Sea, which we have shown to be sensitive to the Atlantic Multidecadal Oscillation, are critical to the formation of Antarctic bottom water[6], an important generator of the thermohaline circulation. The Atlantic Multidecadal Oscillation itself is considered to be the ocean surface response to changes in the thermohaline circulation[21,23]. This raises the possibility that the Atlantic Multidecadal Oscillation directly interacts with the thermohaline circulation in the Southern Ocean. Such an interaction may be important for understanding the climate system on multidecadal and even longer timescales.

METHODS SUMMARY

We used linear regression, MCA decomposition and two numerical models in this study. Statistical confidence levels are shown with linear regression indices, and MCA decomposition identifies the mode that maximizes the covariance between two different variables. The CAM4 response to Atlantic Multidecadal Oscillation SST forcing was obtained as the difference between a control run forced with 1980s boundary conditions and a perturbation run in which only SSTs in the north and tropical Atlantic were modified. The GFDL model shows the dynamical response to an idealized initial perturbation, mimicking the Atlantic Multidecadal Oscillation SST warming.

Online Content Any additional Methods, Extended Data display items and Source Data are available in the online version of the paper; references unique to these sections appear only in the online paper.

1. Vaughan, D. G., Marshall, G. J., Connolley, W. M., King, J. C. & Mulvaney, R. Devil in the detail. *Science* **293,** 1777–1779 (2001).
2. Schneider, D. P., Deser, C. & Okumura, Y. An assessment and interpretation of the observed warming of West Antarctica in the austral spring. *Clim. Dyn.* **38,** 323–347 (2012).
3. Pritchard, H. *et al.* Antarctic ice-sheet loss driven by basal melting of ice shelves. *Nature* **484,** 502–505 (2012).
4. Joughin, I., Alley, R. B. & Holland, D. M. Ice-sheet response of oceanic forcing. *Science* **338,** 1172–1176 (2012).
5. Yuan, X. & Martinson, D. G. The Antarctic dipole and its predictability. *Geophys. Res. Lett.* **28,** 3609–3612 (2001).
6. Holland, P. R. & Kwok, R. Wind-driven trends in Antarctic sea-ice drift. *Nature Geosci.* **5,** 872–875 (2012).
7. Arblaster, J. M. & Meehl, G. A. Contributions of external forcings to southern annular mode trends. *J. Clim.* **19,** 2896–2905 (2006).
8. Karoly, D. J. Southern hemisphere circulation features associated with El Niño-Southern Oscillation events. *J. Clim.* **2,** 1239–1252 (1989).
9. Fogt, R. L., Bromwich, D. H. & Hines, K. M. Understanding the SAM influence on the South Pacific ENSO teleconnection. *Clim. Dyn.* **36,** 1555–1576 (2011).
10. Schlesinger, M. E. & Ramankutty, N. An oscillation in the global climate system of period 65–70 years. *Nature* **367,** 723–726 (1994).
11. Booth, B. B., Dunstone, N. J., Halloran, P. R., Andrews, T. & Bellouin, N. Aerosols implicated as a prime driver of twentieth-century North Atlantic climate variability. *Nature* **484,** 228–232 (2012).
12. King, M. A. *et al.* Lower satellite-gravimetry estimates of Antarctic sea-level contribution. *Nature* **491,** 586–589 (2012).
13. O'Donnell, R., Lewis, N., McIntyre, S. & Condon, J. Improved methods for PCA-based reconstructions: case study using the Steig et al. (2009) Antarctic temperature reconstruction. *J. Clim.* **24,** 2099–2115 (2011).
14. Stammerjohn, S. E., Martinson, D. G., Smith, R. C., Yuan, X. & Rind, D. Trends in Antarctic annual sea ice retreat and advance and their relation to El Niño–Southern Oscillation and Southern Annular Mode variability. *J. Geophys. Res.* **113,** C03S90 (2008).
15. Son, S. W. *et al.* The impact of stratospheric ozone recovery on the Southern Hemisphere westerly jet. *Science* **320,** 1486–1489 (2008).
16. Turner, J. *et al.* Non-annular atmospheric circulation change induced by stratospheric ozone depletion and its role in the recent increase of Antarctic sea ice extent. *Geophys. Res. Lett.* **36,** L08502 (2009).
17. Thompson, D. *et al.* Signatures of the Antarctic ozone hole in Southern Hemisphere surface climate change. *Nature Geosci.* **4,** 741–749 (2011).
18. Marshall, G. J. Trends in the Southern Annular Mode from observations and reanalyses. *J. Clim.* **16,** 4134–4143 (2003).
19. Ding, Q., Steig, E. J., Battisti, D. S. & Küttel, M. Winter warming in West Antarctica caused by central tropical Pacific warming. *Nature Geosci.* **4,** 398–403 (2011).
20. Okumura, Y. M., Schneider, D., Deser, C. & Wilson, R. Decadal–interdecadal climate variability over antarctica and linkages to the tropics: analysis of ice core, instrumental, and tropical proxy data. *J. Clim.* **25,** 7421–7441 (2012).
21. Knight, J. R., Allan, R. J., Folland, C. K., Vellinga, M. & Mann, M. E. A signature of persistent natural thermohaline circulation cycles in observed climate. *Geophys. Res. Lett.* **32,** L20708 (2005).
22. Gray, S. T., Graumlich, L. J., Betancourt, J. L. & Pederson, G. T. A tree-ring based reconstruction of the Atlantic Multidecadal Oscillation since 1567 A.D. *Geophys. Res. Lett.* **31,** L12205 (2004).
23. Zhang, R. & Delworth, T. L. A new method for attributing climate variations over the Atlantic Hurricane Basin's main development region. *Geophys. Res. Lett.* **36,** L06701 (2009).
24. Häkkinen, S., Rhines, P. B. & Worthen, D. L. Atmospheric blocking and Atlantic multidecadal ocean variability. *Science* **334,** 655–659 (2011).
25. Ting, M., Kushnir, Y., Seager, R. & Li, C. Forced and internal twentieth-century SST Trends in the North Atlantic. *J. Clim.* **22,** 1469–1481 (2009).

26. Lefebvre, W. & Goosse, H. Influence of the Southern Annular Mode on the sea ice-ocean system: the role of the thermal and mechanical forcing. *Ocean Sci. Discuss.* **2,** 299–329 (2005).
27. Stammerjohn, S., Massom, R., Rind, D. & Martinson, D. Regions of rapid sea ice change: An inter-hemispheric seasonal comparison. *Geophys. Res. Lett.* **39,** L06501 (2012).
28. Goosse, H. & Zunz, V. Decadal trends in the Antarctic sea ice extent ultimately controlled by ice-ocean feedback. *Cryosphere Discuss.* **7,** 4585–4632 (2013).
29. Bracegirdle, T. J. & Marshall, G. J. The reliability of Antarctic tropospheric pressure and temperature in the latest global reanalyses. *J. Clim.* **25,** 7138–7146 (2012).
30. Bromwich, D. H. *et al.* Central West Antarctica among the most rapidly warming regions on Earth. *Nature Geosci.* **6,** 139–145 (2013).

Author Contributions X.L., D.M.H. and E.P.G. designed the experiments; X.L. performed the data analysis and CAM4 numerical simulations, and prepared all figures; C.Y. ran the initial value calculations; C.Y. and X.L. created Extended Data Fig. 1 and all authors wrote and reviewed the main manuscript text.

METHODS

Data sets. The Modern Era Retrospective analysis for Research and Applications (MERRA) data sets were generated by NASA, using the GEOS-5 Data Assimilation System with a resolution of half a degree by two-thirds of a degree[31]. We used the monthly mean version of MERRA from January 1979 to September 2012, obtained from the NASA Goddard Earth Sciences Data and Information Services Center (http://disc.sci.gsfc.nasa.gov/mdisc/data-holdings). MERRA reanalysis of SLP and SAT (over land only) is shown in Figs 2 and 3.

The ECMWF Interim Re-Analysis (ERA-Interim) was produced by the European Centre for Medium Range Weather Forecasts (ECMWF) using four-dimensional variational assimilation[32]. The resolution of the atmospheric model (IFS Cy31r1/2) is T255 (nominally 0.7 degrees). We used the monthly mean version of ERA-Interim from January 1979 to December 2010, available from the NCAR Computational Information System Laboratory Research Data Archive (http://rda.ucar.edu/datasets/ds627.1/). ERA-Interim reanalysis provides nearly identical results to MERRA, as illustrated in Extended Data Fig. 2.

The UK Met Office (http://www.metoffice.gov.uk/hadobs/hadisst/) Hadley Centre's SIC and SST data set HadISST spans from 1870 to the present[33]. We used the entire period to calculate the Atlantic Multidecadal Oscillation index, and data from 1979 to 2012 for the regression and MCA analysis. There is a discontinuity in HadISST SIC in 2009, owing to the switch of satellite source data at this time. We verified that this did not affect our results in both the linear regression and MCA.

The SAT observations (Fig. 3b) are from 18 Antarctic stations, and are archived by the British Antarctic Survey (http://www.antarctica.ac.uk).

The method established by the NOAA Earth System Research Laboratory was used to calculate the Atlantic Multidecadal Oscillation index (http://www.esrl.noaa.gov/psd/data/timeseries/AMO/). The NOAA Atlantic Multidecadal Oscillation index is calculated from the Kaplan SST dataset (http://www.esrl.noaa.gov/psd/data/gridded/data.kaplan_sst.html). We verified that our calculations based on HadISST are nearly identical (not shown).

Regression and significance level. In Fig. 2, we show both regression coefficients and significance level, which were calculated following ref. 34. Because the degrees of freedom used in the significance calculation are influenced by the autocorrelation of each of these two time series, we adjusted the degrees of freedom following[34]:

$$T^* = T(1 - r_1 r_2)/(1 + r_1 r_2)$$

where T^* is the degree of freedom used in the significance calculation, r_1 and r_2 are the lag-one autocorrelation of each time series, and T is the unadjusted degree of freedom.

In these regressions, we first performed normalization on the time series. The colour contour of the regressions of SLP, SAT and SIC in all of our figures show the regression results against one unit of SST standard deviation. Using Fig. 2a as an example, the colour shading in this panel is the regression of Southern Hemisphere SLP onto the normalized Atlantic SST time series. It shows that a one standard deviation anomaly of Atlantic SSTs (upper left inset) is associated with SLP anomalies of about 200 Pa. We note that whereas the standard deviation of north and tropical Atlantic sub-decadal variability is around 0.2 K, the trend of SSTs during the past 30 years is about half a degree.

MCA decomposition. MCA (also called singular value decomposition) was performed following ref. 35. The strategy of this method is to perform a singular value decomposition of the covariance matrix between the two time series. The spatial patterns of each variable (high dimensional time series) are the singular vectors, and the temporal variability is retrieved by projecting the spatial patterns back onto the original time series. The first mode of MCA maximizes the covariance between the two variables. Thus, the method identifies modes (with spatial and temporal patterns) that both dominate the variability in the two time series and which are strongly correlated with one another.

CAM4 model simulations. The NCAR climate model, the Community Atmosphere Model version 4 (CAM4), is used in this study to verify the teleconnection link and to establish the direction of the causal relationship between Atlantic SST forcing and Antarctic regional climate. CAM4 is the atmospheric component of the Community Earth System Model, CESM 1.0.4. We employ the finite-volume dynamical core of CAM4 with a global horizontal resolution of about 2 degrees. The Community Land Model and the thermodynamic module of the Community Sea-Ice Model are used to estimate the heat flux at the surface, to ensure that the SST is the only external lower-boundary forcing on the atmospheric model.

A control run was forced with monthly varying, annually repeating SST and SIC, and carbon dioxide and ozone concentrations, all fixed at 1980s levels. The SST and SIC annual cycles were obtained by averaging HadISST data over the period 1976–1985. Three forced runs were set up by changing only the SSTs in the north and tropical Atlantic (20° S–70° N), the tropical Atlantic (20° S–20° N), and

the mid-latitude north Atlantic (20° N–70° N). The SST anomalies were imposed following the Atlantic Multidecadal Oscillation SST pattern. To avoid spurious effects at the boundaries, SST anomalies were linearly interpolated to zero over a finite window.

The difference between forced runs and the control run defines the response of the atmospheric model to each SST forcing. All integrations were run for 110 years starting from the same initial conditions, and the results from year 11 to year 110 were used to investigate the model response to the specified SST forcing. Although the atmospheric response to SST anomalies is fairly fast (timescale of a month), long integrations were needed to assess the influence of natural variability and determine the importance of the response.

GFDL model simulations. The idealized model is the spectral dry dynamical core of an atmospheric general circulation model[36–38] from the National Oceanic and Atmospheric Administration (NOAA), developed by the GFDL, and here called the GFDL model. We ran the model with resolution T42 (approximately 3 degrees). The model is initialized with the climatological background flow of the ERA-Interim renalysis[32] for the months of June, July and August from 1979 to 2011. To balance the model with this climatological state, an additional time-independent forcing is added to the model equation at every time step[37–40]. This additional forcing is obtained by integrating the model forward one time step with the initial condition. Until a tropical heating is introduced as an initial perturbation, this additional forcing neutralizes the model's initial tendency, putting the model into a steady state. This procedure ensures that the model response in each time step (or snapshot) is due only to the initial perturbation.

To examine the atmospheric response to tropical Atlantic warming, we construct an idealized convective heating profile that mimics the Atlantic Multidecadal Oscillation SST pattern. The horizontal structure is set to the Atlantic Multidecadal Oscillation SST pattern between 20° S and 20° N (shown in the subpanel of Fig. 2g), to be as similar as possible to the tropical Atlantic CAM4 simulation. The vertical structure of the heating is based on heating observed in deep convection[38,41,42]. The simulation results, however, are insensitive to the details of the horizontal or vertical structure of the heating.

In sum, the GFDL simulation results shown in Extended Data Fig. 1 are the dynamical responses to an initial perturbation mimicking the Atlantic Multidecadal Oscillation SST warming, in different snapshots (from day 3 to day 18, with a three-day interval, after the initial perturbation).

Teleconnection mechanism. We explored the mechanism of this teleconnection by performing two independent model experiments: (1) boundary condition sensitivity experiments using the comprehensive CAM4 model as shown in the 'CAM4 model simulations' section, and (2) initial condition sensitivity experiments using the idealized GFDL model as shown in the 'GFDL model simulations' section. By comparing the simulation results of these two experiments (Extended Data Fig. 1), we discovered that Rossby wave trains directly link the north and tropical Atlantic and Antarctica.

Previous studies have established that a tropical SST warming enhances convection locally, which drives anomalous divergence of the atmospheric flow on the planetary scale[43]. Rossby waves are generated when divergence interacts with the background vorticity gradient[44], and so poleward propagating wave trains appear from the flanks of the subtropical jets[8,41]. It is also known that the propagation of the wave trains depends critically on the background flow[8,9]. The idealized model gives us full control over the background state, and therefore allows us to identify the propagation of Rossby wave trains, excited by tropical Atlantic warming in austral winter.

Extended Data Fig. 1a–f shows the development of Rossby wave trains over the first 18 days after introducing the initial heating perturbation in the GFDL model, at which time the pattern has reached a steady state. We focus on the 200 hPa level, where the wave trains are most pronounced. For reference, we show the climatological 200 hPa geopotential height response of the CAM4 simulation forced by tropical Atlantic SST in Extended Data Fig. 1g. (The surface response of this simulation is shown in Fig. 2g.) In just 2 weeks, the Rossby wave trains generated by tropical Atlantic warming in the idealized atmospheric model (GFDL) propagates to, and focuses on, the Amundsen Sea Low region, generating a pattern comparable to the climatological response of the comprehensive atmospheric model (CAM4).

The idealization of the GFDL atmospheric model used in the initial condition calculations captures only the dry, primitive-equation dynamics of the atmosphere, and hence only the influence of the background state on Rossby wave train propagation. In contrast, the boundary condition calculations in the CAM4 atmospheric model include all atmospheric processes, making the simulation results more realistic. Despite the different physics between these two models, the clear Rossby wave train propagation path (Extended Data Fig. 1a–f) simulated by GFDL initial condition experiments are highly similar (Extended Data Fig. 1f and g) to the result of CAM4 boundary condition experiments. This provides solid evidence

that Rossby wave trains excited by tropical Atlantic convective heating directly link tropical Atlantic warming and Antarctic climate.

To further verify the mechanism, we performed identical simulations with both the idealized GFDL model and comprehensive CAM4 model, but using the austral summer (December, January and February) background state. In both austral summer simulations (not shown), the Rossby wave train is trapped in the sub-tropics and no response is observed in the Amundsen Sea region. This suggests that the teleconnection depends critically on the background state of the atmosphere, and may explain why it is not observed in austral summer.

Teleconnection vertical structure. To illustrate the Antarctic circulation response to Atlantic SST forcing more comprehensively, we display the regression of 200 hPa and 500 hPa geopotential height alongside SLP in Extended Data Fig. 2a–c. These results are also compared with the regression from ERA-Interim data (Extended Data Fig. 2d–f), revealing a strong consistency between these two data sets. We also note that geopotential height and SLP indicate that the circulation response over west Antarctica is quite barotropic, with nearly the same structure from the surface to 200 hPa.

In Extended Data Fig. 2, the tropical Atlantic SST projects a significant signal onto the SLP and geopotential height over the entire tropical region. This global-scale Walker cell anomaly related to the Atlantic SST might also play a part in this teleconnection. The relationship between Walker circulation and the Atlantic–Antarctic teleconnection remains the subject of further study.

Teleconnection seasonality. Our focus is on the austral winter (June, July and August). In the main text, we show only the regressions and simulation results for austral winter, that is, the season in which we have found the most significant statistical (see Extended Data Fig. 3) results from regression and MCA. Here we also show the regression results of SLP onto detrended (and normalized) tropical Atlantic SST time series for each season in Extended Data Fig. 3. In the regression results, warm tropical Atlantic SST deepens the Amundsen Sea Low in all seasons except austral summer (December, January and February).

Tropical versus mid-latitude north Atlantic forcing. To separate the influence of mid-latitude north versus tropical Atlantic SST associated with the Atlantic Multidecadal Oscillation, we performed three forced experiments. An integration forced by anomalies associated with the Atlantic Multidecadal Oscillation ($20°$ S–$70°$ N) is shown in Fig. 2f and an integration forced by anomalies associated with the Atlantic Multidecadal Oscillation restricted to the tropics ($20°$ S–$20°$ N) is shown in Figs 2g and 3c. A third simulation was forced with the Atlantic Multidecadal Oscillation SST anomaly over the mid-latitude North Atlantic alone ($20°$ N–$70°$ N). The three simulations are presented together in Extended Data Fig. 4a–c.

The responses to total north Atlantic (Extended Data Fig. 4a) and tropical Atlantic SST (Extended Data Fig. 4b) forcing show a similar SLP response, whereas the response to the mid-latitude north Atlantic (Extended Data Fig. 4c) forcing exhibits a much weaker SLP response. This implies that the tropical Atlantic has a primary role in the teleconnection between Atlantic SST and Antarctic circulation. The response of SLP in these three experiments is fairly additive, that is, the responses to mid-latitude north Atlantic SST and to tropical Atlantic SST, summed together, are similar to the total response.

The mid-latitude north Atlantic SST warming generates an amplitude in Antarctic Peninsula SAT warming (Extended Data Fig. 4) similar to that of the tropical Atlantic warming, suggesting that the mid-latitude SSTs could still affect Antarctic climate. These atmosphere-only simulations do not account for air–ice–ocean interactions, however, so future study is needed to establish the importance of mid-latitude north Atlantic SSTs.

Southern Annular Mode trend. There are concerns about the fidelity of reanalysis trends in SLP around Antarctica, particularly in the Amundsen Sea Low region, our principal area of focus. First, natural variability is extremely large over this region, so that SLP trends in the reanalysis are not statistically significant. Second, it has been reported that trends in the reanalysis data are biased over the Antarctic region[29]. Different reanalyses do not agree with each other; we find opposite, albeit statistically insignificant, trends in the MERRA and ERA-Interim reanalyses. For these reasons, SLP trends are not shown in the main text.

The pattern correlation between the north and tropical Atlantic–Antarctica teleconnection SLP (Fig. 2a) is correlated ($R = 0.84$) with the SLP pattern associated with the Southern Annular Mode[45]. A proxy for the Southern Annular Mode index has been reconstructed from weather station observations of SLP alone, and suggests a positive, albeit statistically insignificant, trend of the Southern Annular Mode in June, July and August[18]. We show analysis of this Southern Annular Mode index (data available from http://www.nerc-bas.ac.uk/icd/gjma/sam.html) in Extended Data Fig. 5a, b, illustrating the positive, but not statistically significant, trend. Furthermore, on interannual and interdecadal timescales, many other factors have been shown by previous studies to have the potential to drive the Southern Annular Mode, including the ozone loss, the greenhouse gases, the teleconnection with ENSO and so on.

Impact of the tropical Pacific on different timescales. Previous studies have established that tropical Pacific SST can affect the Antarctic climate by Rossby wave propagation (primarily focusing on the impact of ENSO and central Pacific warming)[8,19]. In this study, we introduced a teleconnection between the tropical Atlantic and Antarctic climate with similar dynamics. Therefore it is important to discuss the relative importance of these source regions. We show below that, whereas the Pacific dominates tropical SST variability on interannual timescales, the Atlantic contributes more on interdecadal timescales.

We first highlight the three widely discussed tropical regions in Extended Data Fig. 6a, together with the spatial-mean SST time series and 34-year trends shown in Extended Data Fig. 6b, c. The interannual standard deviation of SST in the Niño3 region, the central Pacific and the tropical Atlantic are approximately 0.75 K, 0.3 K and 0.2 K, respectively.

The interannual standard deviation of the Niño3 region is about 3.5 times that of the tropical Atlantic; its variance is ten times that. Hence, ENSO dominates the Antarctic climate variability associated with tropical SST on interannual timescales[8,9,27]. The decadal trend of tropical Atlantic SST (about 0.5 K), however, is about three times that of Niño3 SST (about -0.16 K, which is not significant).

Central Pacific variability is comparable to that of the tropical Atlantic. The Central Pacific exhibits a warming trend of about 0.2 K, which is statistically significant, but less than half of the trend in the Atlantic. More importantly, however, the central Pacific warming induces a cooling effect over the Antarctic Peninsula and an opposite sign of SIC redistribution compared with observation[19].

Regression 'with trend' and significance of SIC/SAT. In most of our diagnostic analyses, we first remove the linear trend from the raw data. To support our conclusion better, we show the regressions of SLP, SIC and SAT against the raw time series of north and tropical Atlantic SST, respectively, in Extended Data Fig. 7b, c. These regression results are similar to our detrended regression (Fig. 3a), capturing even greater details of the epochal differences (Fig. 3b or Extended Data Fig. 7a).
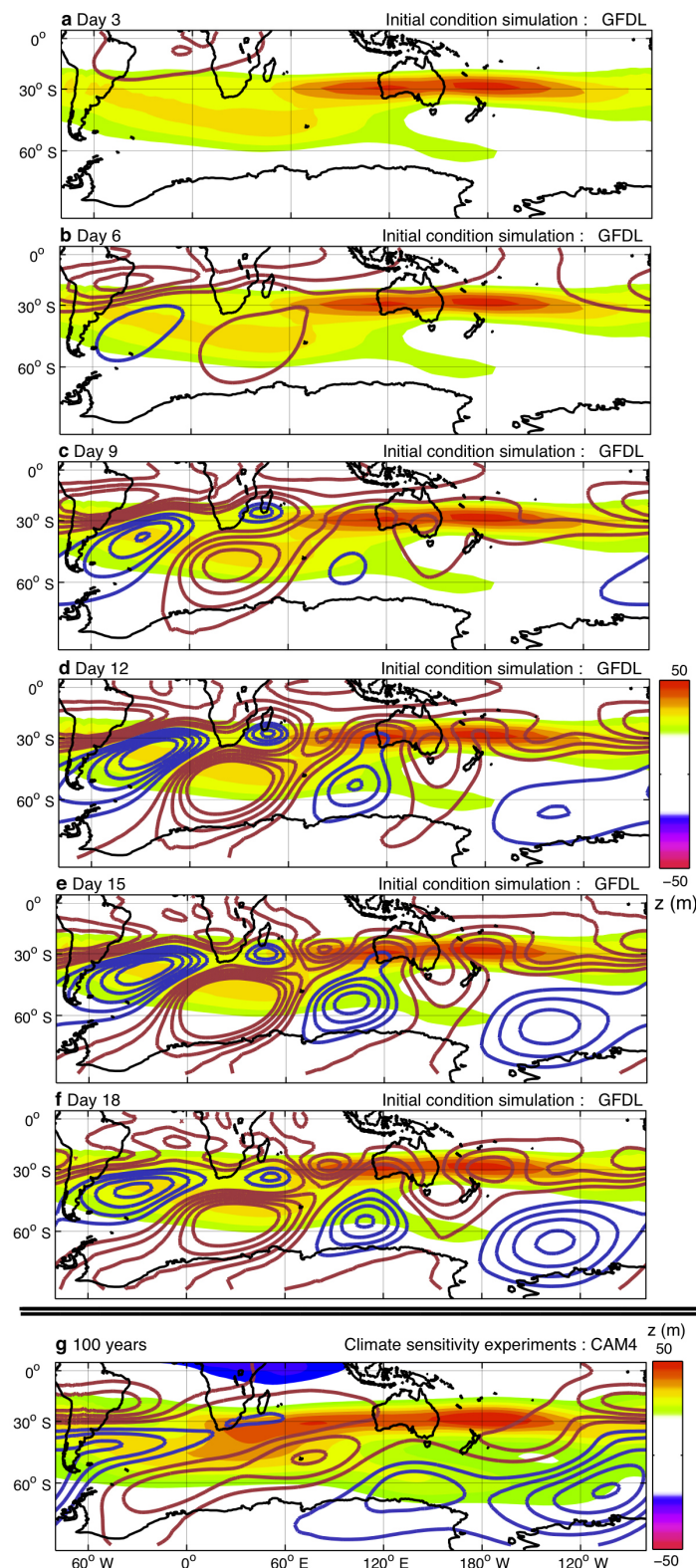
Assessing the statistical significance of the SIC and SAT patterns associated with tropical Atlantic variability is complicated by the limited sample size in the satellite era. Tropical Pacific SSTs associated with ENSO dominate variability in the Atlantic on interannual timescales (Extended Data Fig. 6), making the signal-to-noise ratio associated with Atlantic SSTs weak on these timescales. Hence, the points where the SIC and SAT regression patterns are significant at the 95% level on their own are limited. A point-by-point analysis of the statistical significance, however, ignores information on correlation between different locations, and may lead to an underestimation of the significance level of the whole pattern. The spatial structure of the SIC and SAT regression patterns contains additional information about the teleconnection, which can be used to establish the statistical significance. By spatially averaging the SIC and SAT signals over wider regions, we reduce the noise associated with ENSO variability and establish the significance of the pattern as a whole, as discussed below.

To demonstrate the significance level of the SIC redistribution and the Antarctic Peninsula warming in the observation data, we selected three areas based on the regression result. The red shading in Extended Data Fig. 8 indicates the SIC+ area, where the SIC increases by more than 1% with respect to one standard deviation of tropical Atlantic SST warming in the regression (Fig. 3a). The blue shade indicates the SIC− area, where SIC decreases by more than 1%. SIC is averaged over the above two regions to get the SIC time series of the dipole-like redistribution, whereas the land area inside the grey box (Extended Data Fig. 8) is used to calculate the spatially averaged SAT time series over the Antarctic Peninsula. We performed a Student's t-test for these three regions (against Tropical Atlantic SST time series), and found the P values to be 0.99, 0.97 and 0.95, respectively. All therefore pass the t-test at the 95% confidence level.

The teleconnection between the Atlantic and Antarctica is not based only on this statistical analysis, but is also supported by a clear physical mechanism and numerical simulations with two independent models.
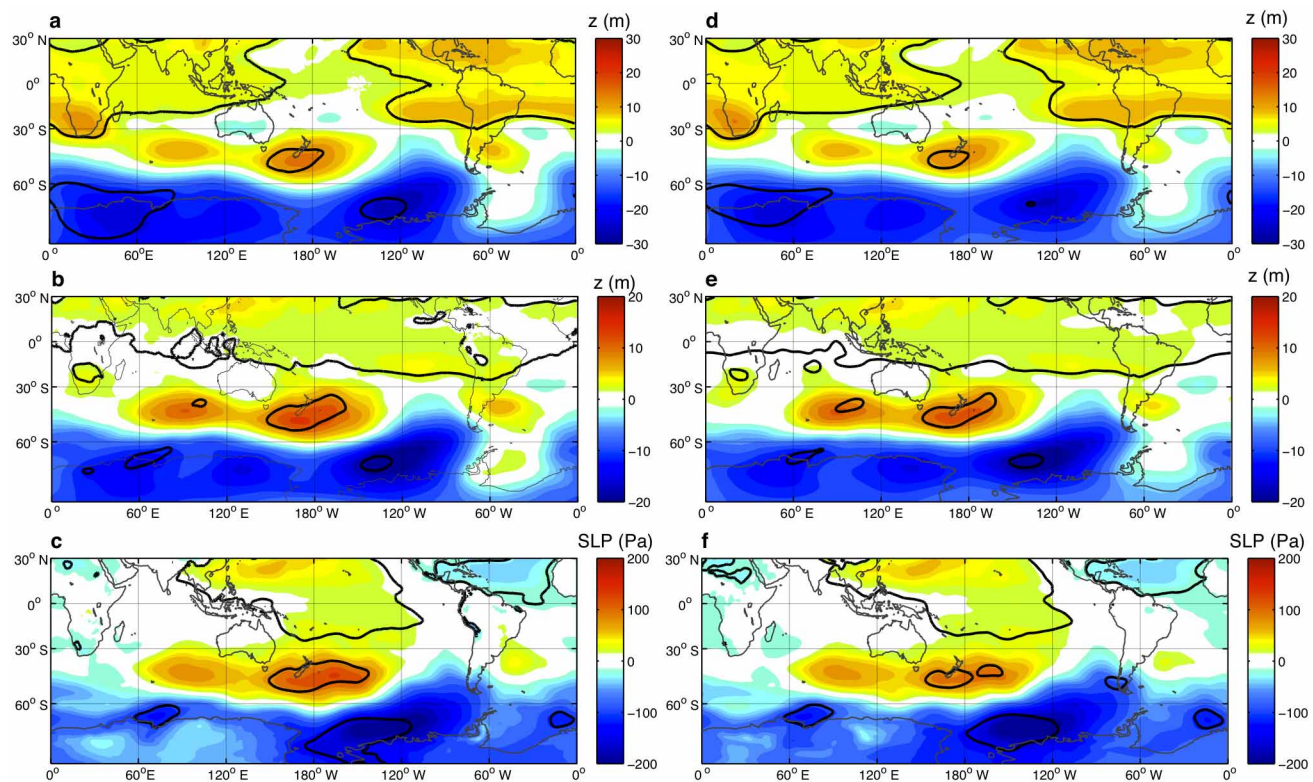
31. Rienecker, M. M. *et al.* MERRA: NASA's modern-era retrospective analysis for research and applications. *J. Clim.* **24,** 3624–3648 (2011).
32. Dee, D. P. *et al.* The ERA-Interim reanalysis: configuration and performance of the data assimilation system. *Q. J. R. Meteorol. Soc.* **137,** 553–597 (2011).
33. Rayner, N. A. *et al.* Global analyses of sea surface temperature, sea ice, and night marine air temperature since the late nineteenth century. *J. Geophys. Res.* **108,** 4407 (2003).
34. Bretherton, C. S., Widmann, M., Dymnikov, V. P., Wallace, J. M. & Bladé, I. The effective number of spatial degrees of freedom of a time-varying field. *J. Clim.* **12,** 1990–2009 (1999).
35. Bretherton, C. S., Smith, C. & Wallace, J. M. An intercomparison of methods for finding coupled patterns in climate data. *J. Clim.* **5,** 541–560 (1992).
36. Held, I. M., Max, J. & Suarez, A. Proposal for the intercomparison of the dynamical cores of atmospheric general circulation models. *Bull. Am. Meteorol. Soc.* **75,** 1825–1830 (1994).

37. Seo, K.-H. & Son, S.-W. The global atmospheric circulation response to tropical diabatic heating associated with the Madden-Julian oscillation during northern winter. *J. Atmos. Sci.* **69,** 79–96 (2012).

38. Yoo, C., Lee, S. & Feldstein, S. B. Arctic response to an MJO-like tropical heating in an idealized GCM. *J. Atmos. Sci.* **69,** 2379–2393 (2012).

39. James, P. M., Fraedrich, K. & James, I. N. Wave-zonal-flow interaction and ultra-low-frequency variability in a simplified global circulation model. *Q. J. R. Meteorol. Soc.* **120,** 1045–1067 (1994).

40. Franzke, C., Lee, S. & Feldstein, S. B. Is the North Atlantic Oscillation a breaking wave? *J. Atmos. Sci.* **61,** 145–160 (2004).

41. Hoskins, B. J. & Karoly, D. J. The steady-state linear response of a spherical atmosphere to thermal and orographic forcing. *J. Atmos. Sci.* **38,** 1179–1196 (1981).

42. Ryu, J.-H., Lee, S. & Son, S.-W. Vertically propagating Kelvin waves and tropical tropopause variability. *J. Atmos. Sci.* **65,** 1817–1837 (2008).

43. Jin, F. & Hoskins, B. J. The direct response to tropical heating in a baroclinic atmosphere. *J. Atmos. Sci.* **52,** 307–319 (1995).

44. Sardeshmukh, P. D. & Hoskins, B. J. The generation of global rotational flow by steady idealized tropical divergence. *J. Atmos. Sci.* **45,** 1228–1251 (1988).

45. Thompson, D. W. J. & Wallace, J. M. Annular modes in the extratropical circulation. Part I: month-to-month variability. *J. Clim.* **13,** 1000–1016 (2000).
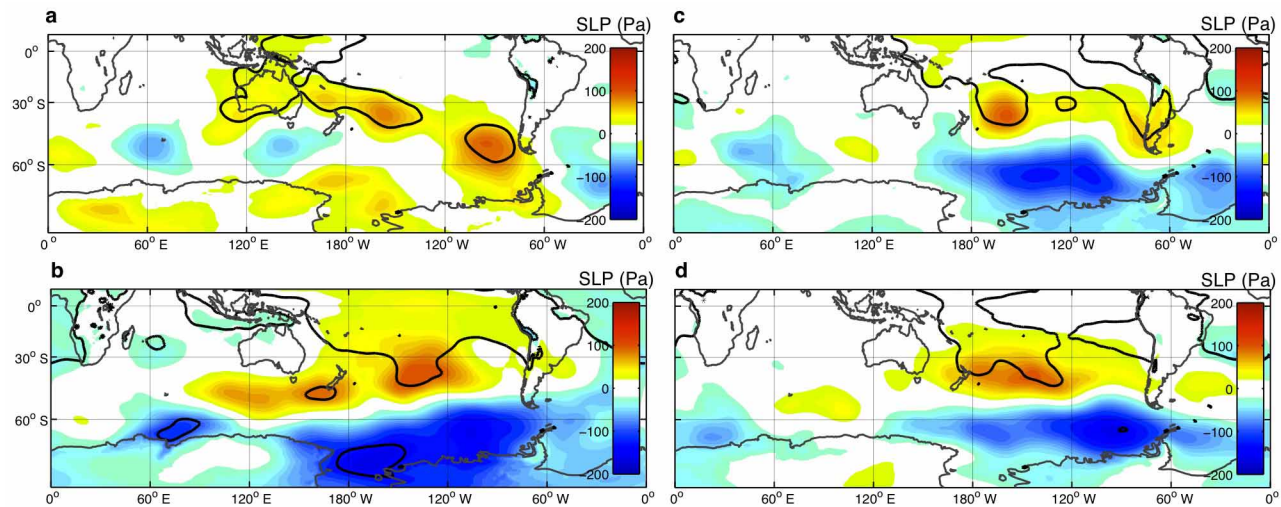
Extended Data Figure 1 | Simulated 200-hPa geopotential height response to tropical Atlantic SST warming in the idealized atmospheric model and comprehensive climate model. Blue (or red) contours at 10-m intervals show negative (or positive) anomalies. Colour shading shows the model's climatological zonal wind on 200 hPa. The strong westerly winds (red regions) mark the sub-tropical jet. In the idealized model, geopotential height (z) anomalies are shown at six different snapshots, from day 3 to day 18 in **a–f** (note that the longitude mapping has been changed to make the tropical Atlantic appear in the upper left corner of each panel). Heating over the tropical Atlantic initially leads to a local increase in geopotential height (**a**, red contour), generating Rossby wave trains that extend poleward (**b**), and then eastward (**c, d**) along the southern edge of the sub-tropical jet. Downstream anomalies appear one by one (**b–e**) and converge on the Amundsen Sea region within two weeks (**e, f**), enhancing the Amundsen Sea Low. The 100-year integration of CAM4 (**g**) shows a similar wave pattern, albeit smoother and with an eastward shift. The resemblance between the initial condition integration (**f**, by GFDL model) and the boundary condition sensitive experiments (**g**, by CAM4) provides evidence that the propagation of Rossby wave trains directly link the tropical Atlantic and Antarctica, in particular, the Amundsen Sea Low area.
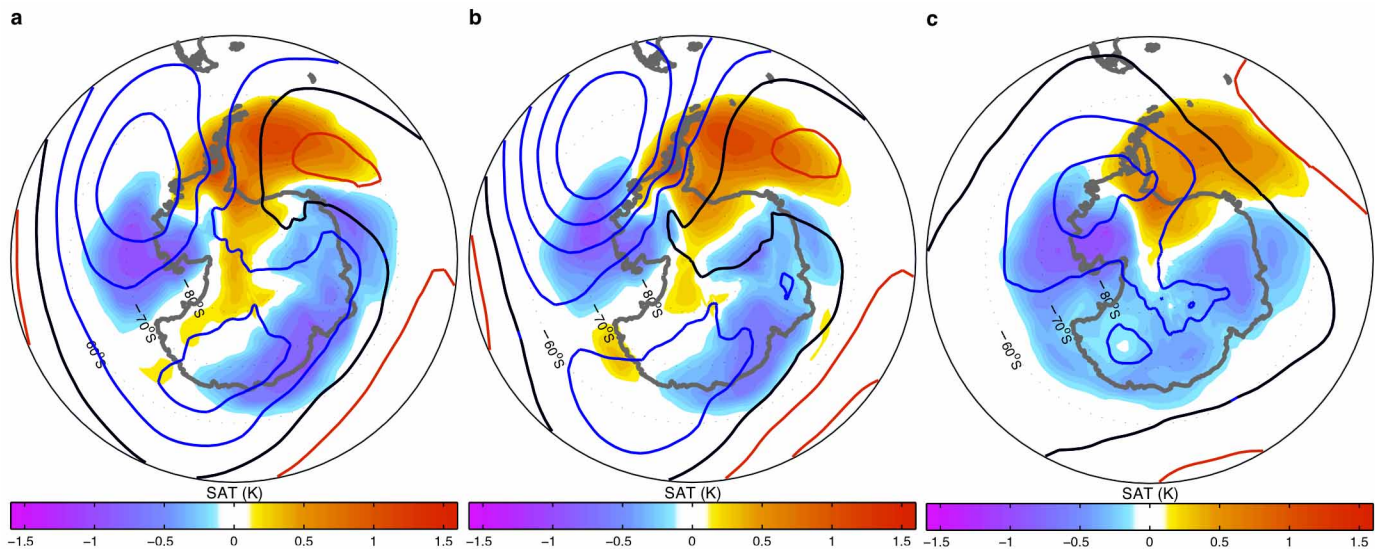
Extended Data Figure 2 | North Atlantic SST projected onto Southern Hemisphere SLP and geopotential height by linear regression, using both MERRA and ERA-Interim data sets. **a–c**, The regression using MERRA data, from 200 hPa (**a**) to the surface (**c**). The main low pressure anomaly centre emerges around Antarctica over the Amundsen–Bellingshausen seas. It is barotropic, from the surface to 200 hPa. **d–f**, The same regressions using ERA-interim data, which show exactly the same phenomena as MERRA. Thick black contours indicate areas with >95% significance.
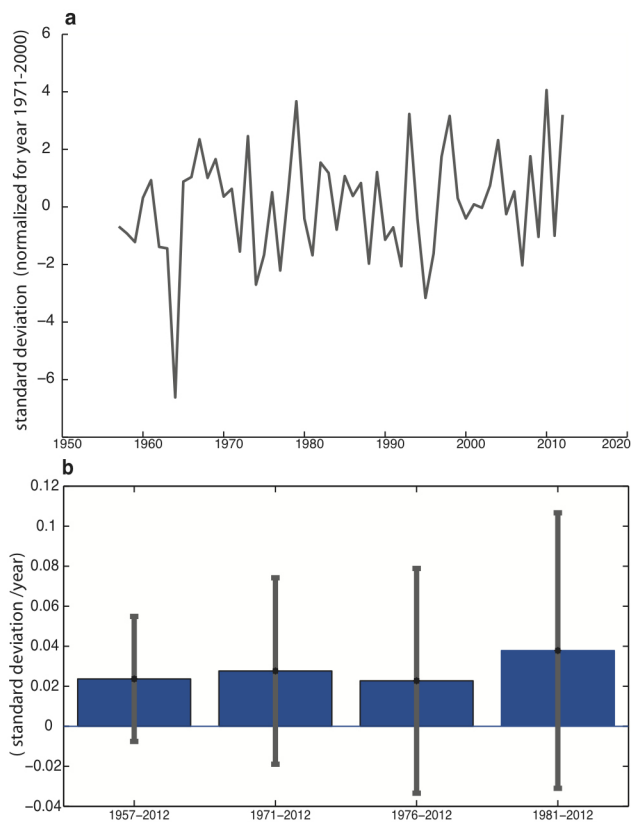
Extended Data Figure 3 | Regression of MERRA sea-level pressure onto detrended Tropical Atlantic sea-surface temperature time series, in all four seasons. **a**, December, January and February; **b**, June, July and August; **c**, March, April and May; and **d**, September, October and November. The Amundsen Sea Low has been deepened in all seasons except in austral summer (December, January and February), and the pattern is most robust in austral winter (June, July and August). Thick black contours indicate areas with >95% significance.
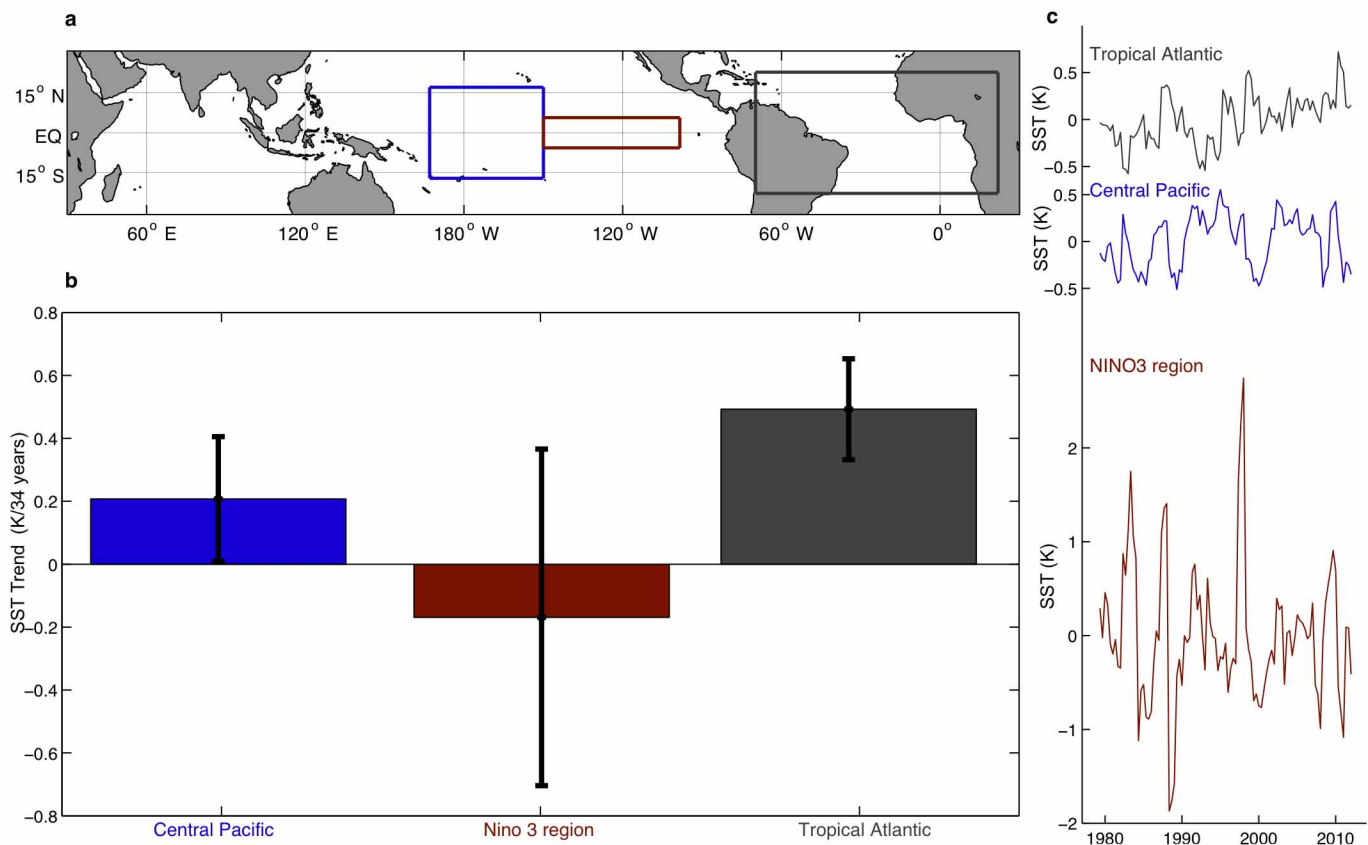
Extended Data Figure 4 | CAM4-simulated Antarctic SLP and SAT with three different SST forcings. a, North Atlantic warming (20° S–70° N); **b,** tropical Atlantic warming (20° S–20° N); and **c,** mid-latitude north Atlantic warming (20° N–70° N). **a** and **b** show a similar SLP response, whereas **c** exhibits a much weaker low-pressure response over west Antarctica, which implies that the tropical Atlantic plays the key part in the teleconnection. The response of SLP in these three experiments show some linearity, whereas the response of SAT is nonlinear. All three experiments, despite having different amplitudes of SLP response, show similar amplitudes of SAT warming/cooling over west Antarctica and the Amundsen–Bellingshausen–Weddell seas. This nonlinearity in SAT response strongly suggests that the impact of mid-latitude north Atlantic SST warming should not be neglected.
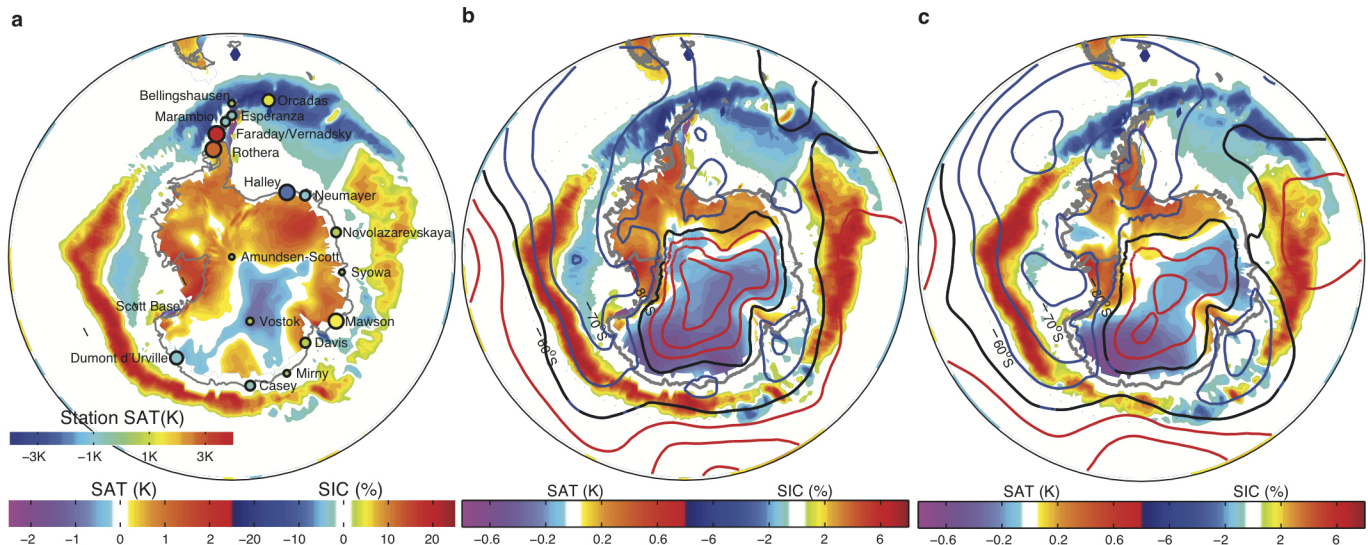
Extended Data Figure 5 | Observed Southern Annular Mode time series and trend in June, July and August. a, The Southern Annular Mode time series in June, July and August since 1957. The data comes from 12 weather stations, compiled by ref. 18. **b**, The linear trend during different periods, all exhibiting a statistically insignificant positive trend. Error bars in **b** indicate the 95% confidence interval (Student's *t*-test).
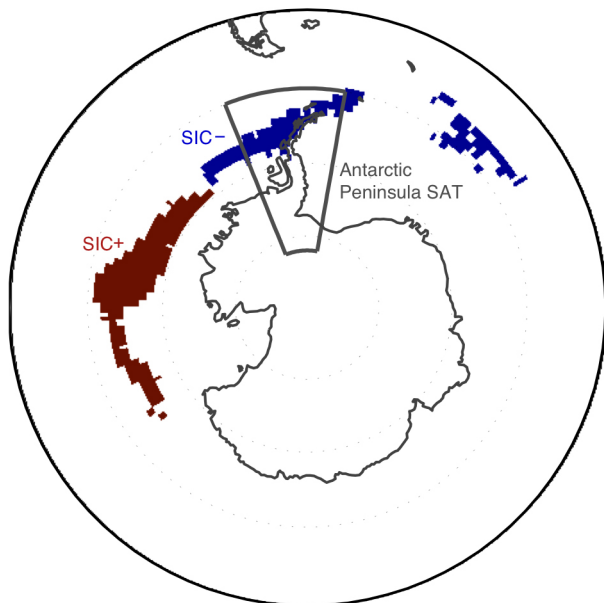
Extended Data Figure 6 | Three tropical regions and their SST trends and variability. a, The blue box indicates the central Pacific area, the red box indicates the Niño 3 region, and the black box indicates the tropical Atlantic region. **b**, SST trend averaged over the three tropical regions in **a**, in June, July and August from 1979 to 2012. The error bars indicate the 95% confidence interval. **c**, The SST time series in June, July and August over these three regions.

Extended Data Figure 7 | Epochal difference and 'with-trend' regression of sea-level pressure, surface air temperature and sea-ice concentration. a, This panel is a duplicate of Fig. 3b and serves as a reference. **b, c**, Regression of SLP, SAT and SIC onto 'with-trend' time series of the north (**b**) and tropical (**c**) Atlantic sub-decadal variability. Both of these show better agreement with the spatial pattern of the epochal difference in **a**; compare with the 'detrended' regression results (Fig. 3a).

Extended Data Figure 8 | Three areas selected to test the significant level of SIC and surface SAT regression. The red shading indicates the area with SIC regression >1% (Fig. 3a), and the blue area shows the SIC regression <−1%. The land area inside the grey box was selected to calculate the spatial-mean SAT over the Antarctic Peninsula. The significance level of the regression is tested over these three areas.